Research Article | Vol. 8, No. 10 | 1 Oct 2017 | BIOMEDICAL OPTICS EXPRESS 4537
Biomedical Optics EXPRESS

Simultaneously extracting multiple parameters via multi-distance and multi-exposure diffuse speckle contrast analysis

JIALIN LIU, HONGCHAO ZHANG, JIAN LU, XIAOWU NI, AND ZHONGHUA SHEN*

School of Science, Nanjing University of Science and Technology, No.200 Xiaolingwei Street, Nanjing 210094, China
*shenzh@njust.edu.cn

Abstract: Recent advancements in diffuse speckle contrast analysis (DSCA) have opened the path for noninvasive acquisition of deep tissue microvasculature blood flow. In fact, in addition to blood flow index αD_B, the variations of tissue optical absorption μ_a, reduced scattering coefficients μ_s', as well as coherence factor β can modulate temporal fluctuations of speckle patterns. In this study, we use multi-distance and multi-exposure DSCA (MDME-DSCA) to simultaneously extract multiple parameters such as μ_a, μ_s', αD_B, and β. The validity of MDME-DSCA has been validated by the simulated data and phantoms experiments. Moreover, as a comparison, the results also show that it is impractical to simultaneously obtain multiple parameters by multi-exposure DSCA (ME-DSCA).

OCIS codes: (170.6480) Spectroscopy, speckle; (300.1030) Absorption; (170.3660) Light propagation in tissues; (290.4210) Multiple scattering.

References and links

1. D. A. Boas, L. E. Campbell, and A. G. Yodh, "Scattering and imaging with diffusing temporal field correlations," Phys. Rev. Lett. **75**(9), 1855–1858 (1995).
2. D. A. Boas and A. G. Yodh, "Spatially varying dynamical properties of turbid media probed with diffusing temporal light correlation," J. Opt. Soc. Am. A **14**(1), 192–215 (1997).
3. R. Bi, J. Dong, and K. Lee, "Deep tissue flowmetry based on diffuse speckle contrast analysis," Opt. Lett. **38**(9), 1401–1403 (2013).
4. R. Bi, J. Dong, and K. Lee, "Multi-channel deep tissue flowmetry based on temporal diffuse speckle contrast analysis," Opt. Express **21**(19), 22854–22861 (2013).
5. R. Bi, J. Dong, C. L. Poh, and K. Lee, "Optical methods for blood perfusion measurement-theoretical comparison among four different modalities," J. Opt. Soc. Am. A **32**(5), 860–866 (2015).
6. C. Yeo, H. C. Park, K. Lee, and C. Song, "Avian embryo monitoring during incubation using multi-channel diffuse speckle contrast analysis," Biomed. Opt. Express **7**(1), 93–98 (2016).
7. M. Seong, Z. Phillips, P. M. Mai, C. Yeo, C. Song, K. Lee, and J. G. Kim, "Simultaneous blood flow and blood oxygenation measurements using a combination of diffuse speckle contrast analysis and near-infrared spectroscopy," J. Biomed. Opt. **21**(2), 027001 (2016).
8. C. Riva, B. Ross, and G. B. Benedek, "Laser doppler measurements of blood flow in capillary tubes and retinal arteries," Invest. Ophthalmol. **11**(11), 936–944 (1972).
9. E. M. Buckley, N. M. Cook, T. Durduran, M. N. Kim, C. Zhou, R. Choe, G. Yu, S. Schultz, C. M. Sehgal, D. J. Licht, P. H. Arger, M. E. Putt, H. H. Hurt, and A. G. Yodh, "Cerebral hemodynamics in preterm infants during positional intervention measured with diffuse correlation spectroscopy and transcranial Doppler ultrasound," Opt. Express **17**(15), 12571–12581 (2009).
10. G. Yu, T. F. Floyd, T. Durduran, C. Zhou, J. Wang, J. A. Detre, and A. G. Yodh, "Validation of diffuse correlation spectroscopy for muscle blood flow with concurrent arterial spin labeled perfusion MRI," Opt. Express **15**(3), 1064–1075 (2007).
11. C. Zhou, S. A. Eucker, T. Durduran, G. Yu, J. Ralston, S. H. Friess, R. N. Ichord, S. S. Margulies, and A. G. Yodh, "Diffuse optical monitoring of hemodynamic changes in piglet brain with closed head injury," J. Biomed. Opt. **14**(3), 034015 (2009).
12. M. N. Kim, T. Durduran, S. Frangos, B. L. Edlow, E. M. Buckley, H. E. Moss, C. Zhou, G. Yu, R. Choe, E. Maloney-Wilensky, R. L. Wolf, M. S. Grady, J. H. Greenberg, J. M. Levine, A. G. Yodh, J. A. Detre, and W. A. Kofke, "Noninvasive measurement of cerebral blood flow and blood oxygenation using near-infrared and diffuse correlation spectroscopies in critically brain-injured adults," Neurocrit. Care **12**(2), 173–180 (2010).

#303782 https://doi.org/10.1364/BOE.8.004537
Journal © 2017 Received 31 Jul 2017; revised 3 Sep 2017; accepted 14 Sep 2017; published 19 Sep 2017

Biomedical Optics EXPRESS

13. M. N. Kim, B. L. Edlow, T. Durduran, S. Frangos, R. C. Mesquita, J. M. Levine, J. H. Greenberg, A. G. Yodh, and J. A. Detre, "Continuous optical monitoring of cerebral hemodynamics during head-of-bed manipulation in brain-injured adults," Neurocrit. Care **20**(3), 443–453 (2014).
14. T. Durduran, R. Choe, G. Yu, C. Zhou, J. C. Tchou, B. J. Czerniecki, and A. G. Yodh, "Diffuse optical measurement of blood flow in breast tumors," Opt. Lett. **30**(21), 2915–2917 (2005).
15. G. Yu, "Near-infrared diffuse correlation spectroscopy in cancer diagnosis and therapy monitoring," J. Biomed. Opt. **17**(1), 010901 (2012).
16. Y. Shang, T. B. Symons, T. Durduran, A. G. Yodh, and G. Yu, "Effects of muscle fiber motion on diffuse correlation spectroscopy blood flow measurements during exercise," Biomed. Opt. Express **1**(2), 500–511 (2010).
17. G. Yu, Y. Shang, Y. Zhao, R. Cheng, L. Dong, and S. P. Saha, "Intraoperative evaluation of revascularization effect on ischemic muscle hemodynamics using near-infrared diffuse optical spectroscopies," J. Biomed. Opt. **16**(2), 027004 (2011).
18. H. Cheng, Q. Luo, S. Zeng, S. Chen, J. Cen, and H. Gong, "Modified laser speckle imaging method with improved spatial resolution," J. Biomed. Opt. **8**(3), 559–564 (2003).
19. J. D. Briers and S. Webster, "Laser speckle contrast analysis (LASCA): a nonscanning, full-field technique for monitoring capillary blood flow," J. Biomed. Opt. **1**(2), 174–179 (1996).
20. D. A. Boas and A. K. Dunn, "Laser speckle contrast imaging in biomedical optics," J. Biomed. Opt. **15**(1), 011109 (2010).
21. D. Briers, D. D. Duncan, E. Hirst, S. J. Kirkpatrick, M. Larsson, W. Steenbergen, T. Stromberg, and O. B. Thompson, "Laser speckle contrast imaging: theoretical and practical limitations," J. Biomed. Opt. **18**(6), 066018 (2013).
22. C. P. Valdes, H. M. Varma, A. K. Kristoffersen, T. Dragojevic, J. P. Culver, and T. Durduran, "Speckle contrast optical spectroscopy, a non-invasive, diffuse optical method for measuring microvascular blood flow in tissue," Biomed. Opt. Express **5**(8), 2769–2784 (2014).
23. H. M. Varma, C. P. Valdes, A. K. Kristoffersen, J. P. Culver, and T. Durduran, "Speckle contrast optical tomography: A new method for deep tissue three-dimensional tomography of blood flow," Biomed. Opt. Express **5**(4), 1275–1289 (2014).
24. Z. Hajjarian and S. K. Nadkarni, "Correction of optical absorption and scattering variations in laser speckle rheology measurements," Opt. Express **22**(6), 6349–6361 (2014).
25. P.-A. Lemieux and D. J. Durian, "Investigating non-Gaussian scattering processes by using nth-order intensity correlation functions," J. Opt. Soc. Am. A **16**(7), 1651–1664 (1999).
26. D. Irwin, L. Dong, Y. Shang, R. Cheng, M. Kudrimoti, S. D. Stevens, and G. Yu, "Influences of tissue absorption and scattering on diffuse correlation spectroscopy blood flow measurements," Biomed. Opt. Express **2**(7), 1969–1985 (2011).
27. P. Farzam and T. Durduran, "Multidistance diffuse correlation spectroscopy for simultaneous estimation of blood flow index and optical properties," J. Biomed. Opt. **20**(5), 055001 (2015).
28. J. Liu, H. Zhang, Z. Shen, J. Lu, and X. Ni, "Quantitatively assessing flow velocity by the slope of the inverse square of the contrast values versus camera exposure time," Opt. Express **22**(16), 19327–19336 (2014).
29. J. Liu, H. Zhang, J. Lu, X. Ni, and Z. Shen, "Quantitative model of diffuse speckle contrast analysis for flow measurement," J. Biomed. Opt. **22**(7), 076016 (2017).
30. A. B. Parthasarathy, W. J. Tom, A. Gopal, X. Zhang, and A. K. Dunn, "Robust flow measurement with multi-exposure speckle imaging," Opt. Express **16**(3), 1975–1989 (2008).
31. A. B. Parthasarathy, S. M. S. Kazmi, and A. K. Dunn, "Quantitative imaging of ischemic stroke through thinned skull in mice with Multi Exposure Speckle Imaging," Biomed. Opt. Express **1**(1), 246–259 (2010).
32. S. M. S. Kazmi, A. B. Parthasarthy, N. E. Song, T. A. Jones, and A. K. Dunn, "Chronic imaging of cortical blood flow using Multi-Exposure Speckle Imaging," J. Cereb. Blood Flow Metab. **33**(6), 798–808 (2013).
33. S. M. S. Kazmi, E. Faraji, M. A. Davis, Y.-Y. Huang, X. J. Zhang, and A. K. Dunn, "Flux or speed? Examining speckle contrast imaging of vascular flows," Biomed. Opt. Express **6**(7), 2588–2608 (2015).
34. W. J. Tom, A. Ponticorvo, and A. K. Dunn, "Efficient processing of laser speckle contrast images," IEEE Trans. Med. Imaging **27**(12), 1728–1738 (2008).
35. T. Durduran, R. Choe, W. B. Baker, and A. G. Yodh, "Diffuse optics for tissue monitoring and tomography," Rep. Prog. Phys. **73**(7), 076701 (2010).
36. R. C. Haskell, L. O. Svaasand, T.-T. Tsay, T.-C. Feng, M. S. McAdams, and B. J. Tromberg, "Boundary conditions for the diffusion equation in radiative transfer," J. Opt. Soc. Am. A **11**(10), 2727–2741 (1994).
37. S. Yuan, "Sensitivity, noise and quantitative model of laser speckle contrast imaging," Ph. D. thesis, Tufts University (2008).
38. R. Michels, F. Foschum, and A. Kienle, "Optical properties of fat emulsions," Opt. Express **16**(8), 5907–5925 (2008).
39. P. Di Ninni, F. Martelli, and G. Zaccanti, "Intralipid: towards a diffuse reference standard for optical tissue phantoms," Phys. Med. Biol. **56**(2), 21–28 (2011).
40. L. Spinelli, M. Botwicz, N. Zolek, M. Kacprzak, D. Milej, P. Sawosz, A. Liebert, U. Weigel, T. Durduran, F. Foschum, A. Kienle, F. Baribeau, S. Leclair, J.-P. Bouchard, I. Noiseux, P. Gallant, O. Mermut, A. Farina, A. Pifferi, A. Torricelli, R. Cubeddu, H.-C. Ho, M. Mazurenka, H. Wabnitz, K. Klauenberg, O. Bodnar, C. Elster, M. Bénazech-Lavoué, Y. Bérubé-Lauzière, F. Lesage, D. Khoptyar, A. A. Subash, S. Andersson-Engels, P. Di

Biomedical Optics EXPRESS

Ninni, F. Martelli, and G. Zaccanti, "Determination of reference values for optical properties of liquid phantoms based on Intralipid and India ink," Biomed. Opt. Express **5**(7), 2037–2053 (2014).
41. P. Di Ninni, F. Martelli, and G. Zaccanti, "The use of India ink in tissue-simulating phantoms," Opt. Express **18**(26), 26854–26865 (2010).
42. B. J. Berne and R. Pecora, *Dynamic Light Scattering: With Applications to Chemistry, Biology, and Physics* (Dover Publications, 2000).
43. L. Dong, L. He, Y. Lin, Y. Shang, and G. Yu, "Simultaneously extracting multiple parameters via fitting one single autocorrelation function curve in diffuse correlation spectroscopy," IEEE Trans. Biomed. Eng. **60**(2), 361–368 (2013).
44. S. Yuan, A. Devor, D. A. Boas, and A. K. Dunn, "Determination of optimal exposure time for imaging of blood flow changes with laser speckle contrast imaging," Appl. Opt. **44**(10), 1823–1830 (2005).
45. S. M. S. Kazmi, S. Balial, and A. K. Dunn, "Optimization of camera exposure durations for multi-exposure speckle imaging of the microcirculation," Biomed. Opt. Express **5**(7), 2157–2171 (2014).
46. S. Sun, B. R. Hayes-Gill, D. He, Y. Zhu, and S. P. Morgan, "Multi-exposure laser speckle contrast imaging using a high frame rate CMOS sensor with a field programmable gate array," Opt. Lett. **40**(20), 4587–4590 (2015).
47. T. Dragojević, D. Bronzi, H. M. Varma, C. P. Valdes, C. Castellvi, F. Villa, A. Tosi, C. Justicia, F. Zappa, and T. Durduran, "High-speed multi-exposure laser speckle contrast imaging with a single-photon counting camera," Biomed. Opt. Express **6**(8), 2865–2876 (2015).
48. A. A. Middleton and D. S. Fisher, "Discrete scatterers and autocorrelations of multiply scattered light," Phys. Rev. B Condens. Matter **43**(7), 5934–5938 (1991).
49. W. B. Baker, A. B. Parthasarathy, D. R. Busch, R. C. Mesquita, J. H. Greenberg, and A. G. Yodh, "Modified Beer-Lambert law for blood flow," Biomed. Opt. Express **5**(11), 4053–4075 (2014).

1. Introduction

Many optical methods, such as diffuse correlation spectroscopy (DCS) [1,2] and diffuse speckle contrast analysis (DSCA) [3–7], have recently been employed for non-invasive blood flow measurements in deep tissues. These methods are usually performed by the illumination of the biological tissue with a coherent light source and detecting the scattered speckle at a certain distance from the light source by a photodetector or camera. The speckle pattern is produced by the coherent addition of the photons experiencing multiple scattering events in tissues with different path lengths. The motion of the scattering particles, mostly red blood cells in vessels, results in the spatial and temporal fluctuations in the light intensity of the speckle pattern. Therefore, these fluctuations can be used to obtain the information about dynamic properties of the red blood cells.

DCS is a recently developed optical method that utilizes the temporal intensity auto-correlation function of speckle pattern to quantify these fluctuations to obtain blood flow in deep tissues. DCS offers some advantages compared with other methods including laser Doppler flowmetry (LDF) [8], Doppler ultrasound [9], perfusion MRI [10], etc. It has been extensively used for various clinical applications such as brain [11–13], cancer [14,15] and muscle [16,17]. Usually, DCS needs a single photon counting avalanche photodiode (APD) to detect the scattered photons and a photon correlator to record the arrival time of the photons detected by the APD. Meanwhile, for improving the signal-to-noise (SNR), multiple APD fibers bundled together in the same position are used to derive an average intensity correlation function. Therefore, DCS is relatively expensive.

As an alternative method, DSCA utilizes the spatial or temporal blurring [18] of speckle pattern defined as speckle contrast for blood flow measurement. DSCA uses the same light source as DCS but with a camera like laser speckle contrast imaging (LSCI) [19–21], i.e. simultaneously capturing many speckles with high frame rates at different distances or exposure times. DSCA has the advantage of simplifying the instrument in hardware and computation process. In fact, DSCA is essentially obtained by the combination of auto-correlation function in DCS and LSCI. We note that it has been demonstrated that the inverse of the speckle contrast ($1/K^2$) has a linear relation with blood flow index (BFI) [3,4]. Besides, some authors [22,23] further demonstrated that it was possible to obtain BFI by the dependence of speckle contrast on exposure time or the source-detector separation. However, these results are all based on the numerical calculation of the time integral over the auto-correlation function. DSCA does not have an analytical expression of speckle contrast like

Biomedical Optics EXPRESS

DCS to describe the influence of optical properties [24] (the absorption μ_a and reduced scattering coefficients μ_s') and BFI on the estimation of speckle contrast. Meanwhile, for extracting a quantitative measurement of BFI from the measurements of speckle contrast, the optical properties of the medium and the coherence factor β [25] depending on the light source and detection optics should be a priori known in DSCA. However, the inaccurate estimations of optical properties can influence the calculated BFI [26]. We note that, recently [27], it has been demonstrated that the multi-distance DCS (MD-DCS) can obtain BFI and optical properties by the dependence of autocorrelation function on the source-detector separations. Therefore, it is necessary to simultaneously extract multiple parameters (BFI, optical properties and a coherence factor β) from DSCA.

In our previous works [28,29], we have deduced an analytical expression of speckle contrast for quantitative flow measurement. This model, combined with multi-exposure speckle imaging (MESI) [30–33] used in LSCI, was fitted to the measured speckle contrasts and the information about BFI was further successfully obtained. In this work, we have deliberately followed the scheme of MD-DCS in Ref [27]. and developed a multi-distance and multi-exposure DSCA (MDME-DSCA) algorithm for simultaneous measurement of multiple parameters by the simulated data and phantom experiments. Besides, we also investigate the possibility of multi-exposure DSCA (ME-DSCA) at a single source-detector (SD) separation for extracting these parameters as a comparison.

2. Methods

2.1 Diffuse speckle contrast analysis (DSCA)

DSCA detects tissue blood flow using the speckle contrast (K) which is defined as the ratio of the standard deviation (σ_s) to the mean intensity ($<I>$) within a local region [34] in the speckle image, i.e. $K = \sigma_s/<I>$. The speckle contrast is related to the normalized electric autocorrelation function $g_1(r,\tau)$ [3,4]:

$$K^2(T) = \frac{2\beta}{T}\int_0^T (1-\tau/T)\left[g_1(r,\tau)\right]^2 d\tau, \tag{1}$$

where T is the camera exposure time, $g_1(r,\tau) = G_1(r,\tau)/G_1(r,0)$, $G_1(r,\tau) = <E(r,t)E^*(r,t+\tau)>$, r is the source-detector (SD) separation, $E(r,t)$ is the light electric field, β is a constant determined by experimental setup and τ is the delay time.

In the multiple scattering media, $G_1(r,\tau)$ is well modeled by the correlation diffusion equation [2,35]

$$\left(-\frac{1}{3\mu_s'}\nabla^2 + \mu_a + \frac{1}{3}\alpha\mu_s' k_0^2 \left\langle \Delta r^2(\tau)\right\rangle\right) G_1(r,\tau) = S(r), \tag{2}$$

where k_0 is the magnitude of the light wave vector in the medium, $S(r)$ is the source light distribution, μ_s' is the reduced scattering coefficient, μ_a is the absorption coefficient, α (0-1) is defined as the fraction of moving scatterers to the total number of scatterers in the medium, and $<\Delta r^2(\tau)>$ is the mean-square displacement (MSD) of the moving scatterers in time τ. Usually, the Brownian motion model $<\Delta r^2(\tau)> = 6D_B\tau$ is considered as a better fit to DCS data than the random flow model, where D_B is the effective Brownian diffusion coefficient of the particles. Therefore, the combined term αD_B is referred to as BFI in tissues, although its unit (cm^2/s) is neither that of flow nor of speed.

The Green's function solution of Eq. (2) for a homogeneous semi-infinite geometry is given by [35]

Biomedical Optics EXPRESS

$$G_1(r,\tau)=\frac{3\mu_s'}{4\pi}\left[\frac{\exp\left(-K(\tau)r_1\right)}{r_1}-\frac{\exp\left(-K(\tau)r_2\right)}{r_2}\right], \tag{3}$$

where $K(\tau)=[3\mu_s'\mu_a+6\mu_s'^2k_0^2\alpha D_B\tau]^{1/2}$, $r_1=[r^2+l_{tr}^2]^{1/2}$, $r_2=[r^2+(l_{tr}+2z_b)^2]^{1/2}$, $z_b=2(1\text{-}R_{eff})/3\mu_s'(1+R_{eff})$, $l_{tr}=1/\mu_s'$, and R_{eff} is the effective reflection coefficient accounting for the index mismatch between the tissue and surrounding medium [36].

In our previous paper [29], we have deduced the general analytical expression of speckle contrast by substituting Eq. (3) into Eq. (1), i.e.

$$\begin{aligned}
K^2(r,T)&=\frac{8\beta}{(FT)^2G_0^2}\sum_{i=1}^{2}\sum_{j=1}^{2}\frac{(-1)^{i+j}}{r_ir_j(r_i+r_j)^4}\left[X_{ij}(T)-X_{ij}(0)+Y_{ij}FT\right],\\
X_{ij}(T)&=\left[(r_i+r_j)^2\left(K_0^2+FT\right)+3(r_i+r_j)\sqrt{K_0^2+FT}+3\right]\times e^{-(r_i+r_j)\sqrt{K_0^2+FT}},\\
Y_{ij}&=\frac{1}{2}(r_i+r_j)^2\left[1+K_0(r_i+r_j)\right]\times e^{-K_0(r_i+r_j)},
\end{aligned} \tag{4}$$

where $K_0=K(\tau=0)=[3\mu_s'\mu_a]^{1/2}$, $F=F=6\mu_s'^2k_0^2\alpha D_B$ and $G_0=4\pi G_1(r,0)/3\mu_s'$. Equation (4) is a rigorous mathematical model of DSCA that describes the typical behavior of speckle contrast K with respect to the absorption μ_a, scattering μ_s' and αD_B at the SD separation r with exposure time T. Typical theoretical $1/K^2$ as a function of αD_B is computed from Eq. (4) by employing the same parameters in Ref [4]. and is plotted in Fig. 1. Our speckle contrast model described by Eq. (4) extends the range over which theoretical $1/K^2$ is linear with αD_B compared with Ref [4]. This linear relation has been studied in our previous works [29]. The analytical solution Eq. (4) can address the underestimation of $1/K^2$ due to the discretization error of the numerical calculation process and provide a physical model for the measured speckle contrasts.

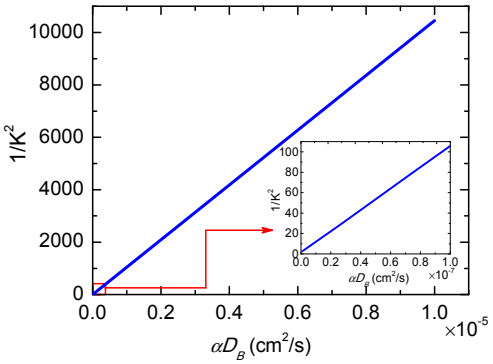

Fig. 1. Theoretical calculation of $1/K^2$ as a function of dynamic parameter αD_B over a broad range. Here $\mu_a=0.03\text{cm}^{-1}$, $\mu_s'=8\text{cm}^{-1}$, $\beta=0.5$, $r=2\text{cm}$, $T=0.2\text{ms}$ and $\lambda=785\text{nm}$ were used.

2.2 Extraction of multiple parameters from multi-distance and multi-exposure DSCA

Multiple parameters (i.e. μ_a, μ_s', αD_B and β) can be obtained by fitting the measured speckle contrasts $K^{measured}(r_i,T_j)$ at multi-distance and multi-exposure to the analytical solution of speckle contrast $K^{theory}(r_i,T_j)$ (see Eq. (4)). The difference between the measured and theoretical speckle contrast, χ^2, is defined as

$$\chi^2=\sum_{i=1}^{N_r}\sum_{j=1}^{N_T}\left[K^{measured}(r_i,T_j)-K^{theory}(r_i,T_j)\right]^2, \tag{5}$$

Biomedical Optics EXPRESS

where r_i is the i'th SD separation, T_j is the j'th exposure time, N_r and N_T are the number of SD separation and exposure time respectively. The goal of MDME-DSCA is to minimize χ^2, which is done by the Nelder-Mead derivative-free simplex method (fminsearch function).

Meanwhile, as a comparison, we also investigate the possibility of obtaining multiple parameters at a single SD separation by the method of multi-exposure DSCA (ME-DSCA). This difference δ^2 is defined as

$$\delta^2 = \sum_{j=1}^{N_r \times N_T} \left[K^{measured}\left(r, T_j\right) - K^{theory}\left(r, T_j\right) \right]^2, \tag{6}$$

where $N_r \times N_T$ is the number of exposure time and equal to the total number of the measured speckle contrasts for MDME-DSCA. We note that the SD separation in the middle of multi-distance used in MDME-DSCA is chosen as a representative for ME-DSCA. Meanwhile, the minimization of this difference δ^2 is also done by fminsearch function.

2.3 Simulated data generation

To test the accuracy of MDME-DSCA and ME-DSCA, we have simulated 125 media with five different absorption (μ_a from 0.04 to 0.16cm^{-1} with a step of 0.03cm^{-1}), five different scattering (μ_s' from 4 to 16cm^{-1} with a step of 3cm^{-1}), and five different αD_B (αD_B from 1.4 × 10^{-8} to 2.6 × 10^{-8}cm^2/s with a step of 0.3 × 10^{-8} cm^2/s). For MDME-DSCA, the same 9 SD separations (r from 0.25 to 1.05cm with a step of 0.1cm) and 10 exposures (T from 0.1 to 1ms with a step of 0.1ms), which were also used for phantom experiments, were used. In a single SD separation fitting for ME-DSCA, 90 exposures from 0.1 to 1ms with a step of 0.01ms at the middle separation r = 0.65cm, where the data at the exposure time T = 0.55ms was removed to have the same number of simulated speckle contrast values as MDME-DSCA, were used. Then these parameters (μ_a, μ_s', and αD_B) were varied to generate simulated speckle contrast values at different exposure time and SD separations using a constant factor β = 0.124 and Eq. (4). The Nelder-Mead derivative-free simplex method was further used to minimize the difference χ^2 or δ^2 to obtain these parameters with the initial values of μ_a, $\mu's$, and αD_B which were randomly assigned (rand function) in the same ranges as those indicated previously, i.e. 0.04≤μ_a≤0.16cm^{-1}, 4≤ μ_s' ≤16cm^{-1}, and 1.4 × 10^{-8}cm^2/s≤αD_B≤2.6 × 10^{-8}cm^2/s. Besides, the initial value of β was randomly determined in the range from 0 to 1, and the termination tolerance for the fitted variables (TolX) was set as 10^{-10} which was enough to obtain precise results for these parameters.

The ability of MDME-DSCA was further examined by fitting the simulated speckle contrasts with the noise. Usually the major noises in DSCA are CCD noise [22,23,37] and statistical noise [37]. The CCD noise is a type of electronic noise and introduces additional background contrast to original speckle contrast. The statistical noise is due to the limited number of pixels used for the calculation of speckle contrast and can cause speckle contrast value fluctuation. Since the CCD noise is not determined by speckle contrast and can be corrected by the method in Ref [22,23], we just generate speckle contrast values with the statistical noise. A mathematical model of statistical noise has been developed in Ref [37]. The model shows that the statistical noise is related to speckle contrast value and increasing the number of pixels can reduce statistical noise. The statistical noise (standard deviation σ_K) of the simulated speckle contrast K is shown as [37]

$$\sigma_K = \frac{K\sqrt{K^2 + 0.5}}{\sqrt{N}}, \tag{7}$$

where N is the number of pixels used for calculating a single speckle contrast value and N = 7 × 7 is the same as the liquid phantom experiments. Therefore, the ratio of the standard deviation σ_K to the speckle contrast K, i.e. σ_K/K, is larger than 0.101.

Biomedical Optics EXPRESS

The standard deviations σ_K corresponding to simulated speckle contrast values at different exposure time and SD separations were calculated by Eq. (7). The noises following a Gaussian distribution with zero mean and standard deviation σ_K were then generated, and added to the simulated speckle contrast values to obtain speckle contrast measurements with noise. Meanwhile, for each exposure time of each SD separation, 1000 speckle contrast values with statistical noise were used to obtain an averaged speckle contrast values like in phantom experiments. Finally the speckle contrast curves with the noise were fitted to simultaneously extract multiple parameters. The discrepancies between the fitted and expected values of the parameters was calculated as [(Fitted-Expected)/Expected] × 100%.

2.4 Tissue simulating phantoms

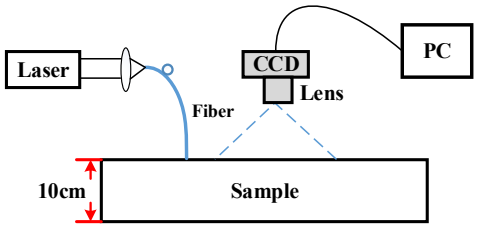

Fig. 2. Schematic of the experimental setup using the phantom.

We have designed the phantom experiments to test the accuracy of MDME-DSCA in homogeneous media. The liquid phantoms comprise of Intralipid [38–40] (30%, Fresenius Kabi, China) for control of the scattering μ_s' and particles Brownian motion αD_B (all particles are considered as dynamic and $\alpha = 1$), India ink [40,41] (Black 4001, Pelikan, Germany) for control of the absorption μ_a, and distilled water. The theory and details of Intralipid including optical properties are described in Ref [38]. The absorption of India ink $\mu_a = 440.1\text{mm}^{-1}$ was measured in our previous work [29]. Then the 30% Intralipid and India ink can be diluted by distilled water to obtain the desired optical properties of the phantoms. As shown in Ref [26], the error in the estimation of αD_B mostly depended on the error in the estimation of the reduced scattering coefficient μ_s' compared with the absorption μ_a. Therefore, MDME-DSCA was validated in five liquid phantoms where μ_s' (4, 7, 10, 13, 16cm^{-1}) was varied, and μ_a = 0.1cm^{-1} and αD_B were constant.

In these MDME-DSCA measurements, we used a long-coherence 671 nm CW laser source (CNI MRL-III-671, 100mW) to illuminate the surface of the phantoms via a 200 μm muti-model optical fiber, and a 12 bit CCD camera (IMC-140F, Imi Tech, Korea) with a lens (f = 50mm and f/# = 8) to record the backscattering speckle patterns as shown in Fig. 2. The imaging region covered the field of view 1.4cm × 1.2cm. We defined nine detector regions with a size of 15 × 15 pixels (0.15 × 0.15mm^2) at different SD separations (r from 0.25 to 1.05cm with a step of 0.1cm). The exposure time ranging from 0.1 to 1ms with a step size of 0.1ms was used and 1000 images were obtained for each exposure time. For each image of each detector region, we used a 7 × 7 window size to calculate the speckle contrast and further obtained a spatially average speckle contrast over the detector region. Then these speckle contrasts were temporally averaged over 1000 images. Besides, we used the method in Ref [22,23]. to correct the influence of CCD noise, i.e. dark and shot noise, on the calculation of speckle contrast. The Nelder-Mead derivative-free simplex method described in Section 2.3 was then used to extract multiple parameters.

Meanwhile, prior to these works, the nanoparticle analyzer, Malvern Zetasizer Nano ZS90, was used to independently measure the particle size distribution of the diluted Intralipid using the dynamic light scattering (DLS) method [42]. The nanoparticle analyzer collected the scattered light at an angle of 90° and obtained Z-average hydrodynamic

Biomedical Optics EXPRESS

diameter D_Z = 195.9 ± 4.7nm from the measured intensity auto-correlation function. Then the particles Brownian motion αD_B can be calculated by the Stokes-Einstein relation

$$\alpha D_B = \frac{k_B T}{3\pi D_Z \eta}, \tag{8}$$

where k_B is the Boltzmann constant, T is the temperature, and η is the viscosity. The viscosity of the phantoms over μ_s' variation at controlled temperature 18 °C was measured by a viscometer, and the particles Brownian motion αD_B can be calculated using the associated viscosity and Eq. (7). The measured viscosity and αD_B were then averaged from five phantoms to obtain η = 1.068 ± 0.023cp and αD_B = (2.04 ± 0.043) × 10^{-8}cm^2/s. We note that the μ_s' variation has minor influence on the viscosity and particles Brownian motion.

3. Results

3.1 Difference patterns in MDME-DSCA and ME-DSCA

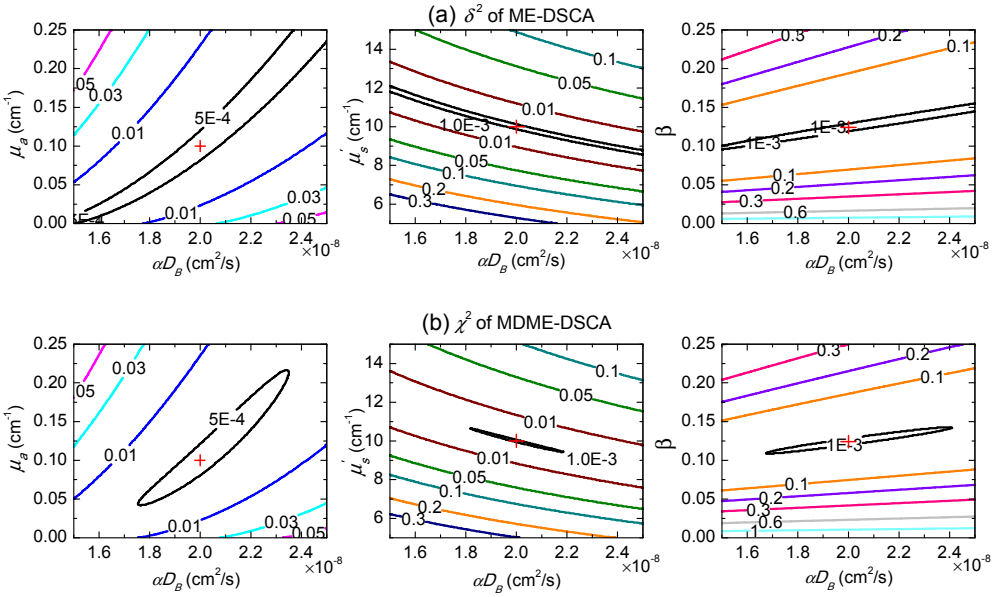

Fig. 3. Contour plots of the differences between the reference (a) ME-DSCA or (b) MDME-DSCA measurements and testing speckle contrast measurements generated by varying the values of paired parameters. The reference speckle contrast measurements were generated by the given parameters μ_a = 0.1cm^{-1}, μ_s' = 10cm^{-1}, αD_B = 2 × 10^{-8}cm^2/s and β = 0.124. χ^2 and δ^2 were obtained by varying the values of $0 \le \mu_a \le 0.25$cm^{-1}, $5 \le \mu_s' \le 15$cm^{-1}, 1.5 × 10^{-8}cm^2/s$\le \alpha D_B \le$2.5 × 10^{-8}cm^2/s and $0 \le \beta \le 0.25$. The reference values of paired parameters are marked at the cross where the differences χ^2 and δ^2 achieve the minimum values.

As shown in Section 2.3, the reference MDME-DSCA and ME-DSCA measurements without noise were generated with the same given parameters: μ_a = 0.1cm^{-1}, μ_s' = 10cm^{-1}, αD_B = 2 × 10^{-8}cm^2/s and β = 0.124. The differences χ^2 and δ^2 between the reference speckle contrast measurements and the testing speckle contrast measurements generated by varying the values of paired parameters, i.e. $0 \le \mu_a \le 0.25$cm^{-1}, $5 \le \mu_s' \le 15$cm^{-1}, 1.5 × 10^{-8}cm^2/s$\le \alpha D_B \le$2.5 × 10^{-8}cm^2/s, and $0 \le \beta \le 0.25$, were calculated by Eq. (5) and Eq. (6) respectively. Contour plots of these differences are then shown for different pairs of parameters in Fig. 3. In the ME-DSCA, the local minima of the difference δ^2 is divergent and has a wide range calculated by the values of paired parameters, which makes it difficult to obtain the minimum at the cross point in Fig. 3(a) using the dependence of speckle contrast on the exposure time. By contrast,

Biomedical Optics EXPRESS

MDME-DSCA confines the local minima of the difference χ^2 to a smaller area and the difference χ^2 is convergent as shown in Fig. 3(b). These results show that it is possible to simultaneously obtain these reference parameters at the cross points by MDME-DSCA. Besides, the curves of the pairs of μ_a and αD_B show that the results of αD_B are less sensitive to μ_a.

3.2 Extraction of multiple parameters from the simulated data

3.2.1 Noise-free simulations

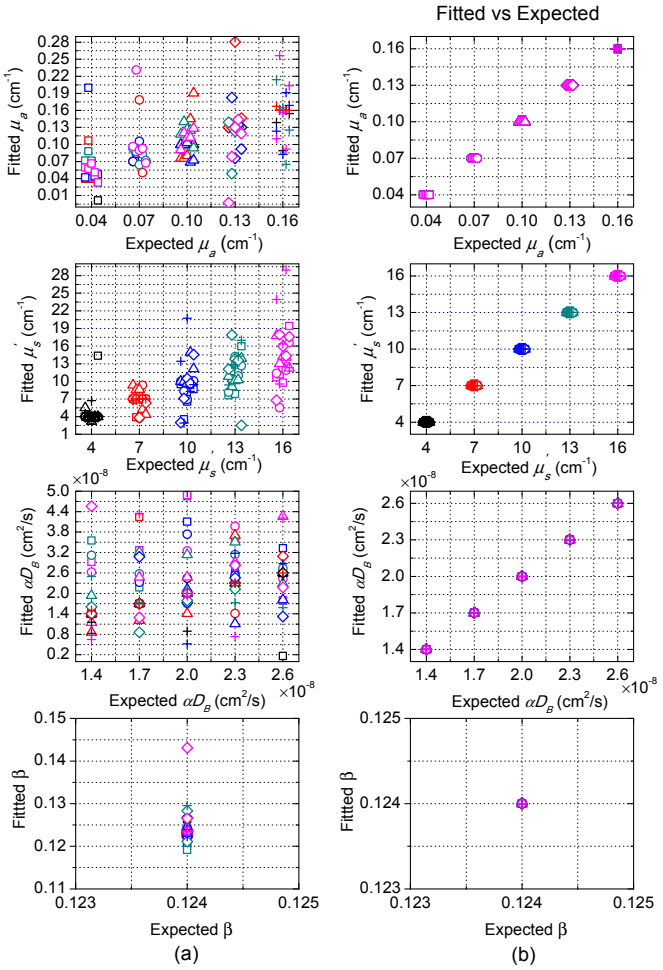

Fig. 4. Fitted parameters μ_a, μ_s', αD_B and β from noise-free data for 125 media by (a) ME-DSCA and (b) MDME-DSCA. The noise-free data for ME-DSCA or MDME-DSCA was generated at the SD separation r = 0.65cm with exposure time T from 0.1 to 1ms with a step of 0.01ms, or at nine SD separations (r from 0.25 to 1.05cm with a step of 0.1cm) with 10 exposures (T from 0.1 to 1ms with a step of 0.1ms). Each marker represents one μ_a, i.e. square: μ_a = 0.04cm^{-1}, circle: μ_a = 0.07cm^{-1}, triangle: μ_a = 0.10cm^{-1}, diamond: μ_a = 0.13cm^{-1}, and cross: μ_a = 0.16cm^{-1}. Each color represents one μ_s', i.e. black: μ_s' = 4cm^{-1}, red: μ_s' = 7cm^{-1}, blue: μ_s' = 10cm^{-1}, dark cyan: μ_s' = 13cm^{-1}, and magenta: μ_s' = 16cm^{-1}. The same marker with different colors means the same μ_a with various μ_s' values. The same color with different markers means the same μ_s' with various μ_a values. For better observing the fitted parameters, we move the points slightly across the x-axis and αD_B increases from left to right for each μ_a or μ_s'.

Biomedical Optics EXPRESS

We have used the Nelder-Mead derivative-free simplex method to simultaneously extract multiple parameters from the simulated ME-DSCA and MDME-DSCA measurements for 125 media as described in Section 2.3. The average number of the iterations was 440 and the average calculation time was 3.14s for the used Intel i5-3450 CPU. Figure 4 shows that the fitted parameters by ME-DSCA have considerable errors even in the noise-free data. These errors are due to the large crosstalk between these parameters. Therefore, it is difficult to decouple the crosstalk by the dependence of speckle contrast on the exposure time. By contrast, MDME-DSCA can accurately obtain all parameters without any error in the noise-free data.

3.2.2 Noise-added simulations

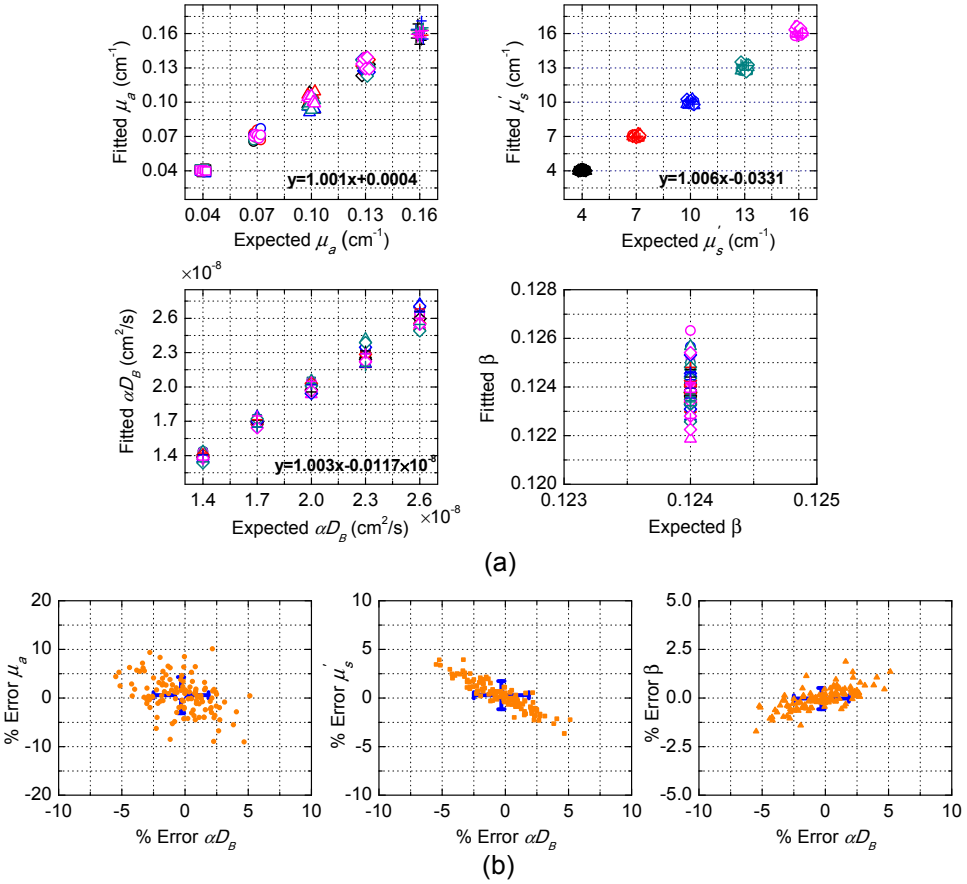

Fig. 5. Performance of MDME-DSCA in the noise-added simulated data. (a) Fitted parameters μ_a, μ_s', αD_B and β, and (b) percentage error of fitted parameters. Each color and marker in (a) represent the same as Fig. 4. The same marker with different colors means the same μ_a with various μ_s' values. The same color with different markers means the same μ_s' with various μ_a values. The linear fitting between fitted parameters and expected parameters is displayed in (a). The percentage error in (b) is defined as [(Fitted-Expected)/Expected] × 100%. The standard deviations of the errors are shown with blue error bars and the centers of the crosses represent the mean values of the errors.

We further verify the feasibility of MDME-DSCA for the noise-added simulated data as shown in Fig. 5. Figure 5(a) shows the estimated multiple parameters from MDME-DSCA and the percentage error of estimated parameters are then calculated as shown in Fig. 5(b). The absolute values of the errors for μ_a, μ_s', αD_B and β are respectively less than 10.11%, 3.94%, 5.48%, and 1.87%. Besides, the mean values and the standard deviations of the errors

Biomedical Optics EXPRESS

are presented as blue error bars in Fig. 5(b). Compared with other parameters, MDME-DSCA may result in a higher error in μ_a. In fact, we can increase the number of speckle patterns to reduce the influence of the noise. In summary, these results show that MDME-DSCA can obtain all parameters from the noise-added simulated data with a relatively high accuracy.

3.3 Extraction of multiple parameters from liquid phantoms data

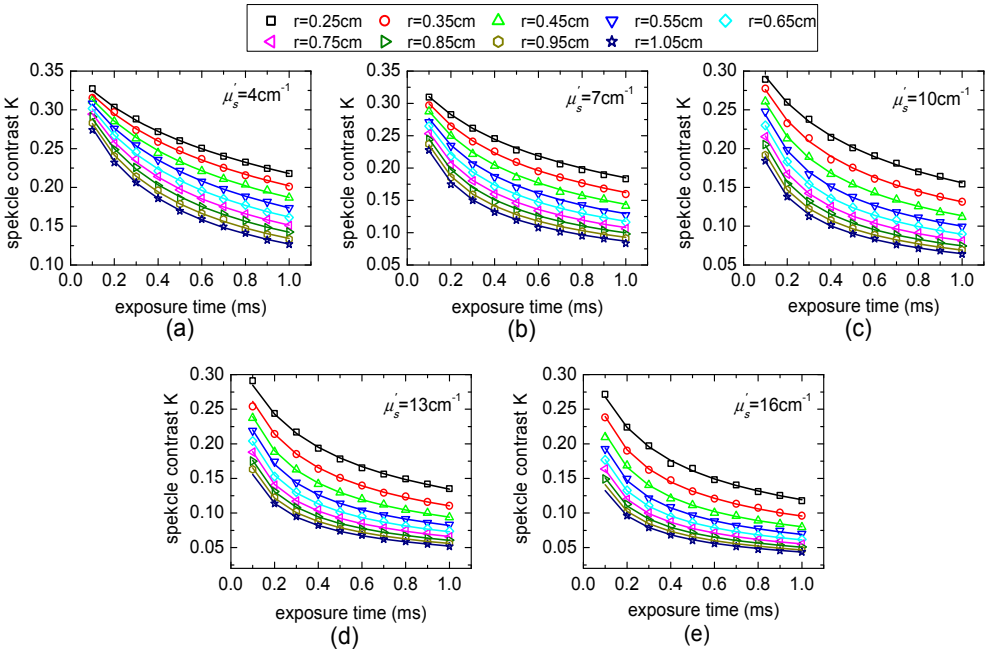

Fig. 6. Speckle contrast measurements from phantom experiments in which μ_s' was varied, i.e. (a) μ_s' = 4cm^{-1}, (b) μ_s' = 7cm^{-1}, (c) μ_s' = 10cm^{-1}, (d) μ_s' = 13cm^{-1}, and (e) μ_s' = 16cm^{-1}, and other parameters were constant. The solid lines are the fitting results calculated by Eq. (4). Some speckle contrast measurements in (d) and (e) are not available due to the low CCD SNR.

Figure 6 shows the speckle contrast measurements from phantom experiments in which μ_s' (4, 7, 10, 13, 16cm^{-1}) was varied and other parameters were constant. The speckle contrast measurements over multiple SD separations for multiple exposure times were calculated by the procedure described in Section 2.4. The solid lines in Fig. 6 represent the calculated speckle contrast curves using Eq. (4) with the fitted parameters in Fig. 7 obtained from MDME-DSCA. We note that the error bars in Fig. 7 are the 95% confidence intervals (CI) of the fitted parameters which are calculated by the nonlinear least-squares regression. The fitted μ_a (0.097 ± 0.020cm^{-1}) and μ_s' are in agreement with the expected value μ_a = 0.1cm^{-1} and expected μ_s'. The Brownian diffusion coefficient αD_B and the factor β are not expected to change along with the varied μ_s', since the change in the viscosity due to the change in μ_s' is negligible and β only depends on light source and detector optics. Indeed, the fitted αD_B (1.93 × 10^{-8} ± 0.16 × 10^{-8}cm^2/s) and β (0.1261 ± 0.004) show good stability, which are in agreement with the priori measurements of αD_B = (2.04 ± 0.043) × 10^{-8}cm^2/s described in Section 2.4 and β = 0.124 estimated from the static speckle contrast.

Biomedical Optics EXPRESS

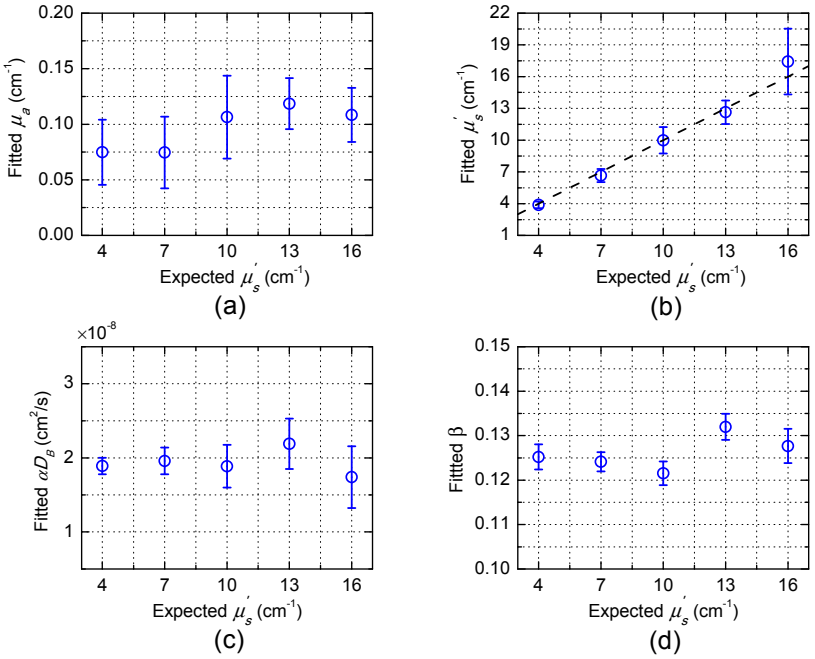

Fig. 7. Fitted parameters (a) μ_a, (b) μ_s', (c) αD_B and (d) β versus the varied μ_s' in the liquid phantoms. The dash line in (b) represents an ideal linear relation with the slope equal to one and intercept equal to zero.

4. Discussion

One of the criticisms for DSCA has been the lack of quantitative speckle contrast model describing the influence of multiple parameters such as μ_a, μ_s', αD_B and β on the speckle contrast measurements. In our previous works [29], the analytical expression of speckle contrast has been used for quantitative αD_B measurement with other known parameters μ_a, μ_s' and β. Due to the facts that the speckle contrast expression is a highly nonlinear function of multiple parameters and the inaccurate measurements of μ_a or μ_s' can lead to incorrect measurements of αD_B, this paper is aimed at separating μ_a, μ_s', αD_B and β from the speckle contrast measurements by this analytical expression. We note that, recently [27], it has been demonstrated that it is possible to use the dependence of autocorrelation function on the SD separations to obtain multiple parameters by multi-distance DCS (MD-DCS). In fact, DSCA is essentially obtained from the combination [3–5] of DCS and laser speckle contrast imaging (LSCI). Therefore, in this paper, we have developed a multi-distance and multi-exposure DSCA (MDME-DSCA) algorithm for simultaneous measurement of multiple parameters. Here, we show that MDME-DSCA can accurately obtain all four parameters without any error in the noise-free simulation data (see Fig. 4). Besides, simultaneous measurements of multiple parameters by MDME-DSCA are also shown to be feasible for the noise-added simulated data (see Fig. 5). Then in order to validate MDME-DSCA, we have performed liquid phantoms experiments. Our experimental results of μ_a, μ_s', αD_B and β agree well with the expected values as shown in Fig. 7. By contrast, it is impractical to simultaneously obtain multiple parameters from multi-exposure DSCA (ME-DSCA) at a single SD separation even in the noise-free simulation data, which is the same as the previous work [43].

Figure 3 well explains these comparison results where it is shown that the minimum differences δ^2 of ME-DSCA has a wide range due to the large cross-talk between these parameters and is divergent. According to the expression of speckle contrast (see Eq. (4)), the decay of speckle contrast depends on αD_B which is only included in the term $FT = 6\mu_s'^2 k_0^2 \alpha D_B T$. It is apparent that it is difficult to separate αD_B and μ_s' using the dependence of speckle

Biomedical Optics EXPRESS

contrast on exposure time T at one SD separation. By contrast, the dependence of speckle contrast on the SD separation makes that the difference χ^2 of MDME-DSCA in Fig. 3 is confined to a smaller area and becomes convergent, suggesting that it is able to use MDME-DSCA to decouple large cross-talk between these parameters.

To further discuss the influence of these parameters on speckle contrast, Fig. 8 shows the dependence of the speckle contrast variation on the μ_s', αD_B and μ_a variation at different SD separations and exposure time. The percentage change in μ_s', αD_B and μ_a are respectively defined as $[(\mu_s' - \mu_{s0}')/\mu_{s0}'] \times 100\%$, $[(\alpha D_B - \alpha D_{B0})/\alpha D_{B0}] \times 100\%$, and $[(\mu_a - \mu_{a0})/\mu_{a0}] \times 100\%$, where $\mu_{s0}' = 10\text{cm}^{-1}$, $\alpha D_{B0} = 2 \times 10^{-8}\text{cm}^2/\text{s}$, and $\mu_{a0} = 0.1\text{cm}^{-1}$ are the same as the given parameters used in Fig. 3. For all variations, the percentage change in K is defined as $[(K(\mu_s', \alpha D_B, \mu_a) - K_0)/K_0] \times 100\%$, where K_0 is obtained from the given parameters μ_{s0}', αD_{B0}, and μ_{a0}. As shown in Fig. 8, for all variations, the variation in K over different SD separations has a wider range compared with the variation in K over different exposure time. On the other hand, the variation in μ_s' in Fig. 8 has a greater influence on the variation in K at both SD separation and exposure time compared with the variation in αD_B. The variation in K due to the variation in μ_a is much less than the variation due to μ_s' or αD_B. Therefore, the differences χ^2 and δ^2 generated by the pair of μ_a and αD_B in Fig. 3 have the biggest area and the fitted μ_a has a higher error from the noise-added simulated data compared with other fitted parameters as shown in Fig. 5.

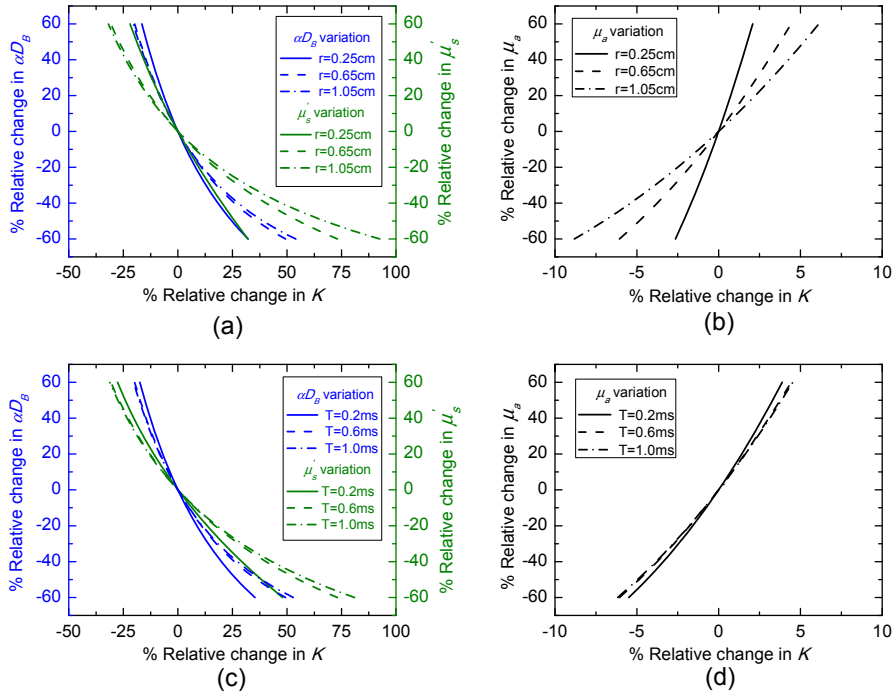

Fig. 8. Variations in μ_s', αD_B and μ_a at different SD separations and exposure time result in corresponding change in speckle contrast. T = 0.6ms was used for the calculation in (a) and (b). r = 0.65 was used in (c) and (d).

Overall, these results show that the reasonable accuracy of MDME-DSCA algorithm opens a relatively low cost, simpler and computationally convenient method for simultaneous extraction of tissue optical properties and dynamic information. Meanwhile, some effects on this method need to be further discussed.

Firstly, the SD separation and exposure time play an important role in MDME-DSCA. We note that DSCA is obtained from a weighted time integral over the autocorrelation function in DCS. However, DSCA is not like DCS to retain fine-details which are retained in the shape of

Biomedical Optics EXPRESS

the measured autocorrelation function in DCS. In this paper we chose 0.25~1.05cm and 0.1~1ms as SD separation and exposure time to capture the dynamic range of the measured speckle contrasts with varied μ_s' as shown in Fig. 6, considering the sensitivity [44,45] of speckle contrast and the signal to noise (SNR). The used SD separations provide a relatively limited measurement of penetration depth as the largest SD separation is 1.05cm. The used exposure time $T = 0.1$ms at SD separation $r = 0.25$cm is used to obtain β, as the speckles have a little de-correlated within this measurement. In fact, the number of exposure time and SD separation could be further increased to improve the accuracy of the fitted parameters. Larger SD separations are required to increase penetration depth of DSCA and smaller exposure time are used to improve the sensitivity to multiple parameters. However, it is difficult to maintain a sufficient SNR at larger SD separation and smaller exposure time. Besides, for shorter SD separations where the diffusion approximation model can't be used, we can also use more advanced models or Monto Carlo simulations to improve the results. These effects should be studied in the future.

A detector region with a size of 15 × 15 pixels (0.15 × 0.15mm^2) as a SD separation in this paper is used to obtain a spatial speckle contrast value. A higher imaging magnification can be used to reduce the size of the detector region, whereas it also reduces the range of SD separation in the CCD field of view. The scanning of the media by moving the camera with a translation stage is a reasonable compromise. Besides, we have used 1000 images for the calculation of the averaged speckle contrast to reduce the statistical errors of speckle contrast. The fast cameras with a high frame rate [46,47] will rapidly reduce the acquisition time of speckle images.

Finally, we note that the autocorrelation function $g_1(r,\tau)$ for a homogeneous semi-infinite geometry is used in this paper and can be simplified to exponential [29] at the early delay-time, i.e. $g_1(r,\tau)\approx\exp[-Fr_1\tau/2(r_1K_0 + 1)]$. The autocorrelation function at early delay-time usually associates with the photons with long light paths in the media [48,49]. $g_1(r,\tau)$ arises from the momentum transfer accumulated by the scattering events of the photons along their paths in the tissue. Usually the photons with long paths undergo a larger number of scattering event and have more momentum transfer, which results in the decay of $g_1(r,\tau)$. This decay due to the photons with long paths is more obvious at early delay-time [48]. Therefore, the speckle contrast at smaller exposure time will be more sensitive to deeper tissue. Besides, the inverse of speckle contrast at larger exposure time can be simplified to a linear equation and the slope of this linear equation could be used to obtain multiple parameters. These works could be included and texted in the future.

5. Conclusion

We have demonstrated the feasibility of simultaneous measurement of multiple parameters (μ_a, μ_s', αD_B and β) by MDME-DSCA. The simulated and experimental results show that using the dependence of speckle contrast on SD separations can well decouple the large cross-talk between these parameters and obtain more accurate estimations of these parameters compared with ME-DSCA. This further makes DSCA a quantitative method for deep tissue blood flow.

Funding

National Natural Science Foundation of China (NSFC) (11174151 and 11274175).

Acknowledgments

We thank Dr. Tao Yan for his support and discussion in function optimization.

Disclosures

The authors declare that there are no conflicts of interest related to this article.